European Radiology (2020) 30:2782–2790
https://doi.org/10.1007/s00330-019-06615-9

BREAST

Comprehensive analyses with radiological and biological markers of breast cancer on contrast-enhanced chest CT: a single center experience using dual-layer spectral detector CT

Jin Il Moon[1] · Bo Hwa Choi[1] · Hye Jin Baek[1] · Kyeong Hwa Ryu[1] · Sung Eun Park[1] · Ji Young Ha[1] · Eun Jung Jung[2] · Han Shin Lee[2] · Hyo Jung An[3]

Received: 16 September 2019 / Revised: 24 November 2019 / Accepted: 11 December 2019 / Published online: 5 February 2020

Abstract

Objectives To evaluate the predictive value of virtual monoenergetic images (VMIs) by assessing tumor conspicuity on dual-layer spectral detector CT (SDCT) and correlate tumor conspicuity on VMI with prognostic biomarkers in patients with breast cancer.

Methods Sixty-four patients underwent arterial phase and 90-s delayed phase dual-layer SDCT. A retrospective tumor conspicuity analysis of 14 benign tumors and 65 breast cancers was performed using conventional images (CIs) and VMI at 40 keV (VMI40) on arterial and delayed phase scans (CI_{ART}, $VMI40_{ART}$, CI_{DE}, $VMI40_{DE}$). Mean Hounsfield units (HU) of tumors were measured on $VMI40_{ART}$ and $VMI40_{DE}$. A receiver operating characteristic (ROC) curve analysis was performed to compare diagnostic accuracy between image sets. Estrogen receptor (ER), progesterone receptor (PR), human epidermal growth factor receptor 2 (HER2), and Ki67 levels were evaluated using histopathology. Correlations between VMI analyses and histological characteristics of cancers were analyzed.

Results Cancers on VMI40 had a significantly higher conspicuity score and mean HU than benign tumors ($p < 0.001$). $VMI40_{DE}$ showed the highest conspicuity for cancers (mean, 3.79) and the greatest area under the ROC curve (0.817; 95% confidence interval 0.745–0.889). $VMI40_{DE}$ yielded significantly higher mean HU for cancers than $VMI40_{ART}$ ($p < 0.001$). The conspicuity score and mean HU on $VMI40_{ART}$ were significantly higher in cancers with ER negativity, PR negativity, and Ki67 positivity ($p < 0.05$).

Conclusions $VMI40_{DE}$ may be useful in the diagnosis of breast cancers due to higher tumor conspicuity and better enhancement than $VMI40_{ART}$. $VMI40_{ART}$ may be beneficial for the prediction of poor breast cancer prognoses.

Key Points

- *VMI40 improved conspicuity of breast cancer than CI.*
- *$VMI40_{DE}$ yielded higher diagnostic performance of breast cancer than $VMI40_{ART}$.*
- *$VMI40_{ART}$ has an additional benefit in terms of prognosis prediction in patients with breast cancers.*

Keywords Biomarkers · Breast neoplasms · Diagnostic imaging · Dual-energy scanned projection radiography · Prognostic factors

Abbreviations

AUC	Area under the receiver operating characteristic curves
CEDM	Contrast-enhanced digital mammography
CET	Contrast-enhanced tomosynthesis
CI	Conventional image

✉ Bo Hwa Choi
iawy82@gmail.com

[1] Department of Radiology, Gyeongsang National University School of Medicine and Gyeongsang National University Changwon Hospital, 11 Samjeongja-ro, Seongsan-gu, Changwon 51472, South Korea

[2] Department of Surgery, Gyeongsang National University School of Medicine and Gyeongsang National University Changwon Hospital, 11 Samjeongja-ro, Seongsan-gu, Changwon 51472, South Korea

[3] Department of Pathology, Gyeongsang National University School of Medicine and Gyeongsang National University Changwon Hospital, 11 Samjeongja-ro, Seongsan-gu, Changwon 51472, South Korea

CTDIvol	CT dose index volume
DLP	Dose length product
ER	Estrogen receptor
HER2	Human epidermal growth factor receptor 2
HU	Hounsfield units
ICC	Intraclass correlation coefficient
keV	Kiloelectron volt
MG	Mammography
PR	Progesterone receptor
ROI	Region of interest
SDCT	Spectral detector CT
TTP	Time-to-peak enhancement
US	Ultrasound
VMI	Virtual monoenergetic image

Introduction

Breast cancer is the second leading cause of female cancer-related deaths, globally [1]. Breast cancers undergo an angiogenesis process, which plays an essential role in tumor growth and metastasis [2, 3]. These new blood vessels are leaky and of poor quality, thereby causing blood to pool around the lesion. Based on this mechanism, iodinated contrast media can improve the visualization of breast cancer. The sensitivity of contrast-enhanced digital mammography (CEDM) and contrast-enhanced tomosynthesis (CET) is not significantly different from breast MRI [4–7]; however, these modalities have limitations in evaluating axillary lymph nodes and can lead to discomfort as a result of breast compression. Contrast-enhanced dedicated breast CT has also been shown to be accurate at identifying breast cancers [8–11]; however, this modality is still limited when it comes to the evaluation of axillary lymph nodes and requires a specific CT vendor.

Recently, virtual monoenergetic images (VMIs), derived from dual-layer spectral detector CT (SDCT) systems, have been found to be clinically useful by improving lesion conspicuity, decreasing artifacts, reducing radiation doses, and material characterization [12]. When used at low kiloelectron volt (keV) levels near the k-edge (33 keV) of iodine, attenuation values are increased tremendously, which improves vascular contrast and lesion conspicuity at a higher quality than conventional imaging [13–16]. To the best of our knowledge, the usability of VMI at low keV derived from dual-layer SDCT for breast cancer has not been investigated. Thus, this investigation aimed to evaluate the predictive value of VMI by assessing tumor conspicuity on dual-layer SDCT and correlate tumor conspicuity on VMI with prognostic biomarkers in patients with breast cancer.

Materials and methods

Patients

The Institutional Review Board of Gyeongsang National University Changwon Hospital approved this retrospective study and waived the requirement for written informed consent. The study population comprised 64 female patients (aged 35 years to 84 years, median age 51 years) who were histopathologically diagnosed with breast cancer and underwent contrast-enhanced chest CT using a dual-layer SDCT system for oncological staging between June 2016 and May 2018. All patients also underwent digital mammography (MG), breast ultrasound (US), and stereotactic or US-guided biopsies of suspicious lesions.

CT protocol

CT was performed on a dual-layer SDCT unit (IQon Spectral CT, Philips Health Systems) with the following scanning parameters: 120 kVp; 33–83 mA; pitch factor, 0.609; rotation time, 0.4 s; collimation, 64 mm × 0.625 mm; slice thickness, 2 mm; slice increment, 2 mm; and smooth filter (filter A). For breast CT scanning in the prone position, an additional pad was prepared and placed on the standard CT table (Fig. 1). Patients lay prone on the padded table and raised both arms while their breasts were positioned within the rectangular hole. From the lower neck to the lower edge of the liver was scanned. A total of 95 mL of iodinated contrast medium (iohexol, Omnipaque 350, GE Healthcare) was injected via a peripheral vein at a rate of 2–2.5 mL/s followed by 43 mL of saline injected at the same rate. Individual contrast injection timing was controlled using bolus tracking in the aortic arch with the threshold set at 150 Hounsfield units (HU) followed by a 10-s delay before arterial phase scanning. Delayed phase

Fig. 1 Additional CT table pad for image acquisition with the patient in the prone position. This pad was placed on the standard CT table for proper spreading of breast tissues when examined. Patients lay prone on the additional table pad, and the patient's breasts were positioned within the rectangular hole

images were obtained 90 s after the initiation of the contrast injection. The average scan time was less than 2 min.

CT post-processing

Conventional images (CIs) were generated by the summation of raw data from the lower and upper layers. All spectral results were displayed in the same manner as CI using commercial software (Spectral Diagnostic Suite, Philips). CIs were reconstructed at 120 kVp and VMIs at 40 keV (VMI40). In the arterial phase, CI (CI_{ART}) and VMI40 ($VMI40_{ART}$) were investigated, and in the 90-s delayed phase, CI (CI_{DE}) and VMI40 ($VMI40_{DE}$) were investigated.

To analyze radiation exposure, the CT dose index volume (CTDIvol) and the dose length product (DLP) were recorded for each CT examination. The effective radiation dose was calculated by multiplying the DLP by a conversion factor (0.014 mSv/mGy·cm) [17, 18].

Lesion conspicuity analysis

Two readers with 4 years of experience in breast imaging and 4 years of experience in musculoskeletal imaging evaluated lesion conspicuity independently in a randomized manner on CI_{ART}, $VMI40_{ART}$, CI_{DE}, and $VMI40_{DE}$. Both were blinded to the final histological results. Conspicuity scores were determined using a 4-point Likert scale (1 = non-diagnostic; 2 = lesion present, features indeterminate; 3 = confidently assessed; 4 = very confidently assessed). For lesions on CT, conspicuity scores represent the visibility of enhancement and may be considered as a marker for the probability of malignancy. The two readers assessed lesion conspicuity in all image sets again after a washout period of 6 months in order to analyze intra-reader agreement.

Quantitative image analysis

Lesion size and mean HU that correlated with US or MG findings were measured on $VMI40_{ART}$ and $VMI40_{DE}$ in the axial plane that showed the maximum dimension and best conspicuity with highest enhancement. Care was taken to avoid areas of necrosis. If no lesion could be identified, regions of interest (ROIs) were manually traced to correspond to the location of the identified lesion on $VMI40_{DE}$. The HU of the pectoralis major muscle were also evaluated by placing circular ROIs on a central slice containing the aortic arch. All measurements were performed twice and averaged. For the relative enhancement ratio calculations, the HU of lesions were divided by the HU of the pectoralis major muscle. Representative cases are shown in Fig. 2.

Histopathological analysis

Histologic reports which evaluated the prognostic biomarker status of the breast cancer were reviewed. Tumor size was divided into two categories (≤ 2 cm or > 2 cm) for statistical analysis. Tumors were graded as 1, 2, or 3 according to the Nottingham scoring system where higher-grade cancers are more aggressive [19, 20]. Tumor grades were then dichotomized into "low" (grades 1 and 2) and "high" (grade 3). Immunohistochemical staining results for estrogen receptor (ER), progesterone receptor (PR), human epidermal growth factor receptor 2 (HER2), and Ki67 were evaluated. The results were dichotomized into "positive" and "negative." For assessing ER and PR, the Allred scoring system was used and a score of more than 2 was considered positive [21]. HER2 overexpression was considered positive when membranes were graded 3+ or 2+ on immunohistochemistry, with HER2 gene amplification in silver-stained in situ hybridization. The Ki67 index was determined to be positive if the expression was 20%. According to the ER, PR, HER2, and Ki67 results, molecular subtypes of breast cancers were classified into "luminal A," "luminal B," "HER2 overexpression," or "triple negative cancer" [22].

Statistical analysis

The conspicuity score of the tumors was expressed in numerical values. Comparisons of conspicuity scores among the four image sets were performed using the Wilcoxon signed-rank test. To compare variables of malignant and benign lesions, the Mann-Whitney *U* test was used in the conspicuity analysis and independent *t* tests were used in the quantitative analysis. Diagnostic accuracy for detecting breast cancers on each image was assessed by calculating the area under the receiver operating characteristic curves (AUC) and the corresponding 95% confidence intervals (95% CIs). The AUCs were compared using the method described by DeLong et al [23]. Comparison tests between conspicuity scores and mean HU and prognostic biomarkers, such as tumor size and grade and ER, PR, HER2, and Ki67 status, were performed using the Mann-Whitney *U* test. Furthermore, conspicuity scores and mean HU among the molecular subtypes of breast cancer were analyzed using the Kruskal-Wallis test. Pairwise comparisons with Bonferroni corrections were performed for significant results. Statistical significance was defined as $p \leq 0.05$. Intra-reader agreement and inter-reader agreement were evaluated using quadratic-weighted Cohen's kappa coefficients (κ) in the conspicuity analysis [24]. To assess inter-reader agreement in the quantitative analysis, we used the intraclass correlation coefficient (ICC) with a two-way random model of consistency [25, 26]. Intra- and inter-reader agreement evaluation included 65 malignant lesions and 14 benign lesions. Data processing and statistical analysis were performed using SPSS

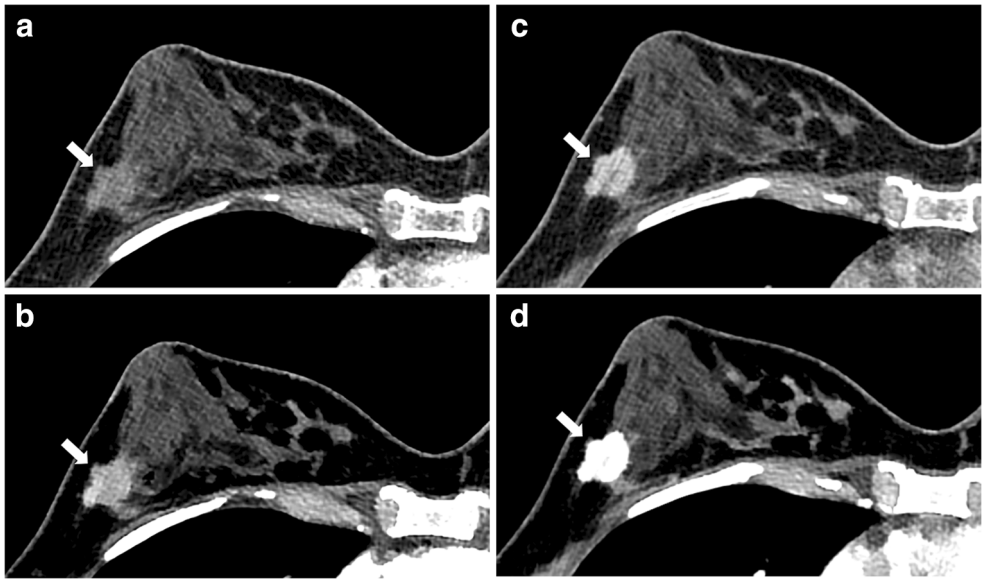

Fig. 2 Images from a 48-year-old woman with invasive ductal carcinoma. **a** Conventional images of arterial phase (CI_{ART}). **b** Virtual monoenergetic image at 40 keV of arterial phase ($VMI40_{ART}$). **c** Conventional images of delayed phase (CI_{DE}). **d** Virtual monoenergetic image at 40 keV of delayed phase ($VMI40_{DE}$). CT images of the right breast show a 2.0-cm irregular enhancing mass (arrows) at 9 o'clock position in all images. Conspicuity scores and mean Hounsfield units (HU) were 2 and 82.9 HU on CI_{ART}, 3 and 116.3 HU on $VMI40_{ART}$, 3 and 148.2 HU on CI_{DE}, and 4 and 361.5 HU on $VMI40_{DE}$. Note that conspicuity scores and mean HU of cancer are the best on $VMI40_{DE}$, due to the high contrast of iodine

(version 24.0, IBM Corp) and MedCalc (version 18.11, MedCalc).

Results

Patients

The characteristics of 64 patients (one patient with bilateral breast cancers) with 65 pathologically proven invasive breast cancers are presented in Table 1. Median age was 51 years (range, 35–84 years). Tumor size ranged from 7.0 to 116.7 mm (mean, 33.2 mm). The median interval between CT and US was 8 days (range, 0–30 days). The average CTDIvol, DLP, and average effective dose of each arterial or delayed phase image were 4.2 mGy (range, 2.9–7.1 mGy), 166.0 mGy·cm (range, 103.5–290.4 mGy·cm), and 2.3 mSv (range, 1.4–4.1 mSv), respectively.

Table 1 Characteristics of 64 women with 65 invasive breast cancers

Characteristics	No. of patients ($N = 64$)
Age, median (range) (years)	51 (35–84)
Stage of initial cancer, no. of patients (%)	
Invasive, stage I	15 (23.4)
Invasive, stage II	27 (42.2)
Invasive, stage III	19 (29.7)
Invasive, stage IV	3 (4.7)
Type of lesion (%) ($N = 65$)	
Invasive ductal carcinoma	56 (86.2)
Mucinous carcinoma	4 (6.2)
Carcinoma with medullary features	3 (4.6)
Invasive lobular carcinoma	1 (1.5)
Carcinoma with neuroendocrine features	1 (1.5)

Lesion conspicuity analysis

The mean conspicuity score of the cancers was significantly higher than that of the benign lesions in all image sets ($p < 0.001$) (Table 2). The conspicuity score of the cancers on delayed phase images (CI_{DE} and $VMI40_{DE}$) was statistically superior to that on arterial phase images (CI_{ART} and $VMI40_{ART}$) ($p < 0.001$). All cancers were detected on delayed phase images by both readers, but six cancers were not detected on arterial phase images. In addition, VMI40 revealed a higher conspicuity score for cancers than CI on arterial and delayed phase images ($p < 0.001$). Of the four image sets, $VMI40_{DE}$ revealed the best depiction of cancers, with a mean conspicuity score of 3.79 (range, 2–4). The AUC of the conspicuity scores for detecting cancers in consensus had the greatest value on $VMI40_{DE}$ (0.817; 95% CI = 0.745, 0.889) (Fig. 3). However, there was no significant difference in AUCs among $VMI40_{DE}$, $VMI40_{ART}$, and CI_{DE} ($p > 0.05$). The AUC of CI_{ART} was significantly lower than that of other image sets ($p < 0.05$). In addition, the overall intra-reader agreement and inter-reader agreement for assessing lesion conspicuity of all image sets were good to excellent

Table 2 Comparative results of tumor conspicuity scores between the four image sets and inter-reader agreement

Conspicuity scoring (1–4)	$VMI40_{ART}$	CI_{ART}	$VMI40_{DE}$	CI_{DE}
Cancer ($N = 65$)	2.74 ± 0.98	1.92 ± 0.81	3.79 ± 0.49	2.71 ± 0.74
Benign ($N = 14$)	1.59 ± 0.80	1.43 ± 0.74	2.64 ± 1.02	1.89 ± 0.71
p value	< 0.001	< 0.001	< 0.001	< 0.001
Intra-reader κ (95% CI)				
Reader 1	0.84 (0.78, 0.90)	0.75 (0.63, 0.86)	0.89 (0.82, 0.96)	0.79 (0.69, 0.88)
Reader 2	0.71 (0.62, 0.81)	0.61 (0.45, 0.76)	0.66 (0.50, 0.83)	0.67 (0.56, 0.79)
Inter-reader κ (95% CI)	0.81 (0.75, 0.86)	0.66 (0.57, 0.74)	0.81 (0.72, 0.90)	0.69 (0.61, 0.77)

Data represent the mean ± standard deviation. p values were calculated using the Mann-Whitney U test

CI confidence interval, CI_{ART} conventional images of arterial phase, CI_{DE} conventional images of delayed phase, $VMI40_{ART}$ virtual monoenergetic image at 40 keV of arterial phase, $VMI40_{DE}$ virtual monoenergetic image at 40 keV of delayed phase

(κ = 0.61–0.89, $p < 0.001$) and the inter-reader agreement for VMI40 was higher than that for CI, regardless of scan timing (Table 2).

Quantitative image analysis

ROIs ranged in size from 18.1 to 4085.3 mm^2 (mean, 437.5 mm^2). The mean HU of the cancers was significantly higher than that of the benign lesions on $VMI40_{ART}$ and $VMI40_{DE}$ ($p < 0.001$) (Table 3). Cancers had significantly higher attenuation values on $VMI40_{DE}$ than on $VMI40_{ART}$ ($p < 0.001$). A similar tendency was shown in the relative enhancement ratios. The AUC of the mean HU for detecting breast cancer in consensus was 0.828 (95% CI = 0.760, 0.883) on $VMI40_{ART}$ and 0.766 (95% CI = 0.720, 0.852) on $VMI40_{DE}$, with no significant difference between the two ($p = 0.325$) (Fig. 4). The ICC values for inter-reader agreement indicated excellent agreement on both $VMI40_{ART}$ (ICC = 0.914, $p < 0.001$) and $VMI40_{DE}$ (ICC = 0.943, $p < 0.001$).

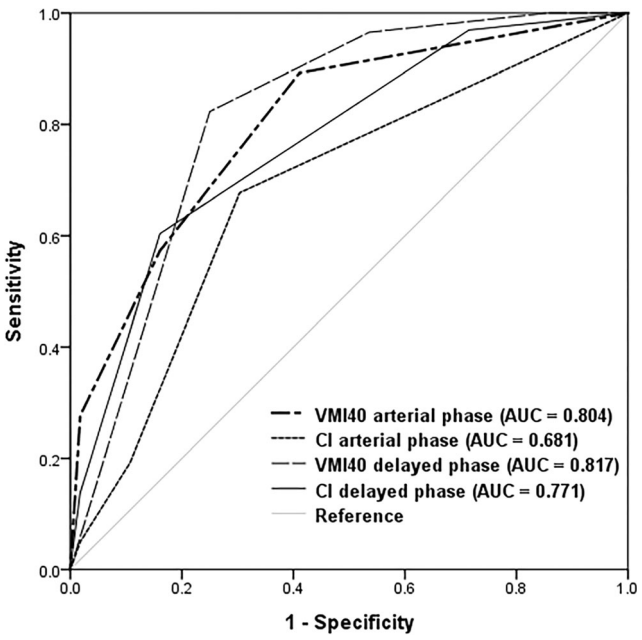

Fig. 3 Comparison of areas under the curve for diagnostic accuracy according to conspicuity scores of tumors in each image set. *AUC* the area under the receiver operating characteristic curves, *CI* conventional images, *VMI40* virtual monoenergetic image at 40 keV

Correlation between VMI analysis and prognostic biomarkers

The conspicuity score on $VMI40_{ART}$ was significantly higher in cancers with a diameter > 2 cm, a high histologic tumor grade, ER negativity, PR negativity, HER2 positivity, and Ki67 positivity ($p < 0.05$) (Table 4). The mean HU of cancers on $VMI40_{ART}$ was significantly higher in cancers with a diameter > 2 cm, ER negativity, PR negativity, and Ki67 positivity ($p < 0.05$) (Table 4). The mean HU of cancers was higher in cancers with HER2 positivity than in those with HER2 negativity with borderline significance on $VMI40_{ART}$ ($p = 0.052$). Histologic tumor grade did not show any significant differences in the mean HU between cancers on $VMI40_{ART}$ ($p = 0.280$). In addition, there was no significant correlation between any prognostic factors and conspicuity scores and the mean HU of cancers on $VMI40_{DE}$ ($p > 0.05$).

Correlation between VMI analysis and molecular subtypes of breast cancer

Conspicuity scores and mean HU of cancers on $VMI40_{ART}$ significantly differed across the four molecular subtypes ($p < 0.001$ for conspicuity scores and $p = 0.020$ for mean HU) (Table 5). Luminal A cancers showed a

Table 3 Comparative results of mean Hounsfield units of the tumors for $VMI40_{ART}$ and $VMI40_{DE}$

	$VMI40_{ART}$ (HU)	*p* value*	$VMI40_{DE}$ (HU)	*p* value†	*p* value‡
Cancer ($N = 65$)	97.4 ± 46.3	< 0.001	201.0 ± 63.5	< 0.001	< 0.001
Benign ($N = 14$)	48.0 ± 31.7	–	117.4 ± 79.0	–	< 0.001
Cancer/muscle	2.2 ± 1.3	< 0.001	2.8 ± 1.1	< 0.001	< 0.001
Benign/muscle	0.9 ± 0.5	–	1.4 ± 0.9	–	0.005

Data represent the mean ± standard deviation. Two readers evaluated images in consensus

HU Hounsfield units, *$VMI40_{ART}$* virtual monoenergetic image at 40 keV of arterial phase, *$VMI40_{DE}$* virtual monoenergetic image at 40 keV of delayed phase

*p values indicate comparisons between benign lesions and cancers on $VMI40_{ART}$

† p values indicate comparisons between benign lesions and cancers on $VMI40_{DE}$

‡ p values indicate comparisons between variables on $VMI40_{ART}$ and $VMI40_{DE}$

significantly lower conspicuity score than luminal B, HER2 overexpression, and triple negative cancers on $VMI40_{ART}$ ($p \leq 0.002$ for all). Moreover, triple negative cancers had a significantly higher conspicuity score than luminal B cancers on $VMI40_{ART}$ ($p = 0.005$). There was no significant difference in cancer conspicuity between HER2 overexpression and triple negative cancers on $VMI40_{ART}$. Regarding mean HU, triple negative cancers had a significantly higher mean HU than luminal A cancers on $VMI40_{ART}$ ($p = 0.037$). There was no significant difference in mean HU between other subtypes of cancers on $VMI40_{ART}$. However, there was no significant correlation between conspicuity scores or mean HU of cancers on $VMI40_{DE}$ and molecular subtypes of breast cancers ($p > 0.05$).

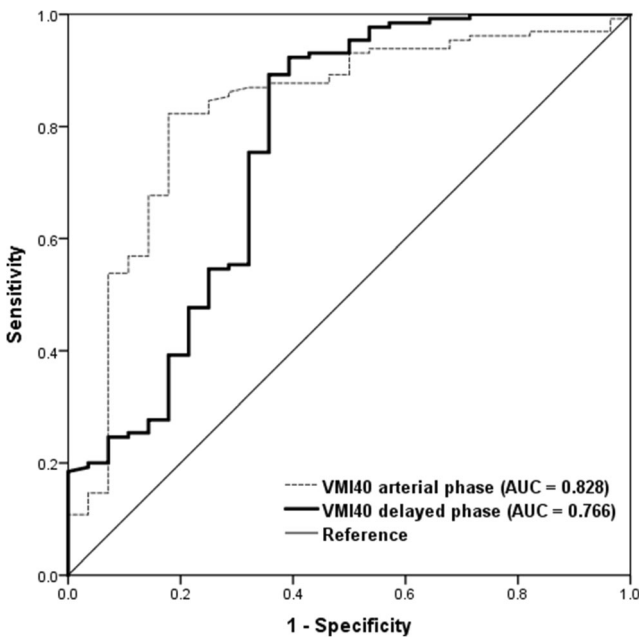

Fig. 4 Comparison of areas under the curve for diagnostic accuracy according to mean Hounsfield units of tumors in each image set. *AUC* the area under the receiver operating characteristic curves, *VMI40* virtual monoenergetic image at 40 keV

Discussion

The preliminary results demonstrate the possibility of a breast cancer diagnosis using contrast-enhanced dual-layer SDCT with VMI40. $VMI40_{DE}$ demonstrates the greatest diagnostic performance among four image sets. In addition, poorer prognostic factors correlated with higher conspicuity and mean attenuation only on $VMI40_{ART}$, indicating an additional benefit of $VMI40_{ART}$ in predicting the prognosis of patients with breast cancer.

VMIs at low keV offer a potential additional modality in oncologic imaging by increasing the iodine enhancement of cancers. A recent study demonstrated that conspicuity and iodine enhancement of breast cancers were significantly higher at VMI40 than at other energy levels (60 keV, 80 keV, and 100 keV) [14]. Regarding scan timing, one previous report demonstrated that 90-s delayed phase scans represent the best scan time to show peak enhancement of breast cancers [27]. Based on these previous studies, the purpose of this investigation was to evaluate the usefulness of VMI40 compared to CI and to demonstrate the clinical feasibility of the 90-s delayed phase scan in patients with breast cancer compared to arterial phase scan. The results showed that $VMI40_{DE}$ yielded the highest conspicuity and mean HU for cancers with the greatest AUC among all image sets. It is noteworthy that all cancers were detected on $VMI40_{DE}$, but that six cancers were not visualized on $VMI40_{ART}$. $VMI40_{DE}$ thus appears to be the best protocol for the detection of breast cancers among the four image sets tested here.

In this study, significant correlations between prognostic factors and cancer conspicuity on $VMI40_{ART}$ were demonstrated. Recently, Park et al [28] investigated the quantification of breast cancer vascularity using low-dose perfusion CT.

Table 4 Correlations of conspicuity scores and mean Hounsfield units of cancers on VMI with prognostic biomarkers

Cancer ($N = 65$)	CS VMI40$_{DE}$	p value	CS VMI40$_{ART}$	p value	HU VMI40$_{DE}$	p value	HU VMI40$_{ART}$	p value
Tumor size								
≤ 2 cm ($N = 19$)	3.74 ± 0.47	0.273	2.43 ± 1.02	0.001	190.4 ± 68.0	0.224	77.2 ± 40.6	0.001
> 2 cm ($N = 46$)	3.81 ± 0.49		2.87 ± 0.94		205.3 ± 61.4		105.8 ± 46.1	
Tumor grade								
Low ($N = 43$)	3.80 ± 0.47	0.710	2.55 ± 0.96	< 0.001	208.5 ± 67.7	0.058	94.3 ± 47.8	0.280
High ($N = 22$)	3.77 ± 0.52		3.11 ± 0.93		186.3 ± 51.8		103.6 ± 43.1	
ER								
Positive ($N = 47$)	3.76 ± 0.52	0.041	2.53 ± 0.97	< 0.001	200.7 ± 68.5	0.917	91.0 ± 46.7	0.011
Negative ($N = 18$)	3.88 ± 0.37		3.29 ± 0.80		201.8 ± 49.0		114.1 ± 41.3	
PR								
Positive ($N = 39$)	3.76 ± 0.51	0.299	2.46 ± 0.95	< 0.001	198.2 ± 61.7	0.552	88.6 ± 42.4	0.007
Negative ($N = 26$)	3.83 ± 0.45		3.17 ± 0.88		205.0 ± 66.4		110.6 ± 49.1	
HER2								
Positive ($N = 20$)	3.79 ± 0.52	0.983	2.95 ± 0.90	0.023	207.8 ± 60.8	0.414	109.2 ± 47.7	0.052
Negative ($N = 45$)	3.79 ± 0.47		2.65 ± 1.05		197.9 ± 64.7		92.1 ± 44.9	
Ki67								
Positive ($N = 49$)	3.80 ± 0.47	0.468	2.91 ± 0.92	< 0.001	201.5 ± 63.4	0.876	103.4 ± 47.2	0.009
Negative ($N = 16$)	3.75 ± 0.53		2.20 ± 0.98		199.4.7 ± 64.6		79.1 ± 38.6	

Data represent the mean ± standard deviation. p values indicate comparisons between two groups using the Mann-Whitney U test

CS conspicuity score, *ER* estrogen receptor, *HER2* human epidermal growth factor receptor 2, *HU* Hounsfield units, *PR* progesterone receptor, *VMI40$_{ART}$* virtual monoenergetic image at 40 keV of arterial phase, *VMI40$_{DE}$* virtual monoenergetic image at 40 keV of delayed phase

They showed that perfusion was significantly higher and time-to-peak enhancement (TTP) was significantly shorter in cancers with high-grade, ER negativity, PR negativity, and HER2 positivity [28]. In summary, poor prognostic cancers show higher perfusion and short TTP. This could explain why cancers with poorer prognostic factors demonstrated earlier enhancement (i.e., arterial phase) with higher mean HU in this study. No correlation between attenuation value of cancers and prognostic factors was found on VMI40$_{DE}$, and it was assumed that cancer enhancement on VMI40$_{DE}$ was too boosted to distinguish the prognostic characteristics of breast cancers.

The usefulness of CT in breast imaging has been limited by radiation dose considerations. While MRI has the highest sensitivity for detecting breast cancers without radiation exposure, barriers to its widespread use include the high cost, the relatively long scanning time, and contraindications related to the administration of gadolinium-based contrast material. Recently, abbreviated breast MRI has been proposed as a faster alternative, but this method still needs a MRI system and the scan time is longer compared to CT [29]. The average scan time of the CT protocol used in this investigation was less than 2 min; thus, most patients did not complain of inconvenience while in the prone position. Furthermore, the average effective dose was 2.3 mSv for each phase, which is very low compared with standard chest CT (7 mSv) [30]. Although two-view digital mammography can be performed with low average effective doses (0.44 mSv), dense breast tissue may obscure cancers, decreasing the sensitivity of mammography [31, 32]. The sensitivity of breast cancers on contrast-enhanced CT may not be affected by breast density. Chest CT is often used in the preoperative evaluation of patients with

Table 5 Correlations of conspicuity scores and mean Hounsfield units of cancers on VMI with molecular subtypes of breast cancer

Cancer ($N = 65$)	CS VMI40$_{DE}$	CS VMI40$_{ART}$	HU VMI40$_{DE}$	HU VMI40$_{ART}$
Luminal A ($N = 16$)	3.75 ± 0.53	2.20 ± 0.98	199.4 ± 64.6	79.1 ± 38.6
Luminal B ($N = 31$)	3.76 ± 0.52	2.70 ± 0.92	201.3 ± 70.9	97.2 ± 49.6
HER2 overexpression ($N = 8$)	3.81 ± 0.47	3.34 ± 0.83	202.0 ± 54.0	114.1 ± 47.6
Triple negative ($N = 10$)	3.93 ± 0.27	3.25 ± 0.78	201.6 ± 46.0	114.0 ± 36.7
p value	0.251	< 0.001	0.999	0.020

CS conspicuity score, *HER2* human epidermal growth factor receptor 2, *HU* Hounsfield units, *VMI40$_{ART}$* virtual monoenergetic image at 40 keV of arterial phase, *VMI40$_{DE}$* virtual monoenergetic image at 40 keV of delayed phase

clinical stage IIIA and higher locoregional disease [33]. One previous study, analyzing the value of preoperative chest CT in patients with primary breast cancer, showed that asymptomatic lung metastases were detected in 0.2%, 0%, and 5.3% of patients with stage I, II, and III disease. Moreover, several studies suggested contrast-enhanced CT as a useful imaging modality to diagnose invasive or in situ breast cancer [10, 11, 34–37]. Therefore, contrast-enhanced dual-layer SDCT could be an alternative imaging modality, especially in patients with contraindications to MRI and in patients with breast cancer of a stage higher than III. Due to recent breakthroughs in artificial intelligence and new techniques such as different X-ray filters for radiation dose reduction, it is expected that the application of these advanced technique could allow breast CT to be performed with high accuracy and reasonable radiation exposure.

This study has several limitations. It is limited by its retrospective, single-center design and the relatively small number of patients with benign or malignant lesions. Further studies using larger sample sizes should be conducted to generalize our results. Secondly, due to the lack of data for comparison with MRI, future studies need to determine whether the diagnostic performance of dual-layer SDCT is comparable to that of breast MRI. Thirdly, HU measurements of cancers were based on an assessment of the index lesion rather than all tumor foci. The approach taken to trace ROIs manually may have resulted in bias. In particular, although we tried to draw the same ROI on $VMI40_{ART}$ by referring to the same image cut on $VMI40_{DE}$ if cancers were not visible on $VMI40_{ART}$, the selection and position of ROIs were still subjective. This may have caused limited sampling in this study. Finally, as one specific machine was used, the results cannot be generalized. Thus, further studies using different dual-energy CT machines and reconstruction algorithms are warranted to investigate the advantages and disadvantages of each setting in more detail.

In conclusion, $VMI40_{DE}$ may be useful for diagnostic use, as it can improve the conspicuity of breast cancer with better contrast enhancement than CI. In addition, $VMI40_{ART}$ has an additional benefit in terms of prognosis prediction. The presented analysis provides a step forward in the effort to improve the image quality of breast CT, thereby making CT an image tool option for detecting breast cancer in patients who cannot undergo breast MRI.

Funding information The authors state that this work has not received any funding.

Compliance with ethical standards

Guarantor The scientific guarantor of this publication is Bo Hwa Choi.

Conflict of interest The authors declare that they have no competing interests.

Statistics and biometry One of the authors has significant statistical expertise. No complex statistical methods were necessary for this paper.

Informed consent Written informed consent was waived by the institutional review board.

Ethical approval Institutional review board approval was obtained.

Methodology
- Retrospective
- Diagnostic or prognostic study
- Performed at one institution

References

1. Ghoncheh M, Pournamdar Z, Salehiniya H (2016) Incidence and mortality and epidemiology of breast cancer in the world. Asian Pac J Cancer Prev 17:43–46
2. Carmeliet P, Jain RK (2000) Angiogenesis in cancer and other diseases. Nature 407:249
3. Weidner N, Semple JP, Welch WR, Folkman J (1991) Tumor angiogenesis and metastasis—correlation in invasive breast carcinoma. N Engl J Med 324:1–8
4. Lewin JM, Isaacs PK, Vance V, Larke FJ (2003) Dual-energy contrast-enhanced digital subtraction mammography: feasibility. Radiology 229:261–268
5. Dromain C, Thibault F, Muller S et al (2011) Dual-energy contrast-enhanced digital mammography: initial clinical results. Eur Radiol 21:565–574
6. Samei E, Saunders RS (2011) Dual-energy contrast-enhanced breast tomosynthesis: optimization of beam quality for dose and image quality. Phys Med Biol 56:6359
7. Chou C, Lewin JM, Chiang C et al (2015) Clinical evaluation of contrast-enhanced digital mammography and contrast enhanced tomosynthesis—comparison to contrast-enhanced breast MRI. Eur J Radiol 84:2501–2508
8. Seifert P, Conover D, Zhang Y et al (2014) Evaluation of malignant breast lesions in the diagnostic setting with cone beam breast computed tomography (breast CT): feasibility study. Breast J 20:364–374
9. Prionas ND, Lindfors KK, Ray S et al (2010) Contrast-enhanced dedicated breast CT: initial clinical experience. Radiology 256:714–723
10. He N, Wu Y, Kong Y et al (2016) The utility of breast cone-beam computed tomography, ultrasound, and digital mammography for detecting malignant breast tumors: a prospective study with 212 patients. Eur J Radiol 85:392–403
11. Aminololama-Shakeri S, Abbey CK, Gazi P et al (2016) Differentiation of ductal carcinoma in-situ from benign microcalcifications by dedicated breast computed tomography. Eur J Radiol 85:297–303
12. Dilmanian FA, Wu XY, Parsons EC et al (1997) Single-and dual-energy CT with monochromatic synchrotron x-rays. Phys Med Biol 42:371–387
13. Doerner J, Hauger M, Hickethier T et al (2017) Image quality evaluation of dual-layer spectral detector CT of the chest and comparison with conventional CT imaging. Eur J Radiol 93:52–58
14. Metin Y, Metin NO, Ozdemir O, Tasci F, Kul S (2019) The role of low keV virtual monochromatic imaging in increasing the conspicuity of primary breast cancer in dual-energy spectral thoracic CT examination for staging purposes. Acta Radiol. https://doi.org/10.1177/0284185119858040

15. Hickethier T, Byrtus J, Hauger M et al (2018) Utilization of virtual mono-energetic images (MonoE) derived from a dual-layer spectral detector CT (SDCT) for the assessment of abdominal arteries in venous contrast phase scans. Eur J Radiol 99:28–33
16. Lee SM, Kim SH, Ahn SJ, Kang HJ, Kang JH, Han JK (2018) Virtual monoenergetic dual-layer, dual-energy CT enterography: optimization of keV settings and its added value for Crohn's disease. Eur Radiol 28:2525–2534
17. Huda W, Ogden KM, Khorasani MR (2008) Converting dose-length product to effective dose at CT. Radiology 248:995–1003
18. Bongartz G, Golding S, Jurik A et al (2000) European guidelines on quality criteria for computed tomography (EUR16262). European Commission, Luxembourg
19. Genestie C, Zafrani B, Asselain B et al (1998) Comparison of the prognostic value of scarff-bloom-Richardson and Nottingham histological grades in a series of 825 cases of breast cancer: major importance of the mitotic count as a component of both grading systems. Anticancer Res 18:571–576
20. Rakha EA, El-Sayed ME, Lee AH et al (2008) Prognostic significance of Nottingham histologic grade in invasive breast carcinoma. J Clin Oncol 26:3153–3158
21. Hammond MEH, Hayes DF, Dowsett M et al (2010) American Society of Clinical Oncology/College of American Pathologists guideline recommendations for immunohistochemical testing of estrogen and progesterone receptors in breast cancer (unabridged version). Arch Pathol Lab Med 134:e48–e72
22. Goldhirsch A, Winer EP, Coates A et al (2013) Personalizing the treatment of women with early breast cancer: highlights of the st gallen international expert consensus on the primary therapy of early breast cancer 2013. Ann Oncol 24:2206–2223
23. DeLong ER, DeLong DM, Clarke-Pearson DL (1988) Comparing the areas under two or more correlated receiver operating characteristic curves: a nonparametric approach. Biometrics 44:837–845
24. Cohen J (1968) Weighted kappa: nominal scale agreement provision for scaled disagreement or partial credit. Psychol Bull 70:213
25. Albrecht MH, Trommer J, Wichmann JL et al (2016) Comprehensive comparison of virtual monoenergetic and linearly blended reconstruction techniques in third-generation dual-source dual-energy computed tomography angiography of the thorax and abdomen. Invest Radiol 51:582–590
26. Lin LI (1989) A concordance correlation coefficient to evaluate reproducibility. Biometrics 45:255–268
27. Seo BK, Pisano ED, Cho KR, Cho PK, Lee JY, Kim SJ (2005) Low-dose multidetector dynamic CT in the breast: preliminary study. Clin Imaging 29:172–178
28. Park EK, Seo BK, Kwon M et al (2019) Low-dose perfusion computed tomography for breast cancer to quantify tumor vascularity: correlation with prognostic biomarkers. Invest Radiol 54:273–281
29. Kuhl CK, Schrading S, Strobel K, Schild HH, Hilgers RD, Bieling HB (2014) Abbreviated breast magnetic resonance imaging (MRI): first postcontrast subtracted images and maximum-intensity projection—a novel approach to breast cancer screening with MRI. J Clin Oncol 32:2304–2310
30. Mettler FA Jr, Huda W, Yoshizumi TT, Mahesh M (2008) Effective doses in radiology and diagnostic nuclear medicine: a catalog. Radiology 248:254–263
31. Hendrick RE (2010) Radiation doses and cancer risks from breast imaging studies. Radiology 257:246–253
32. Suzuki A, Kuriyama S, Kawai M et al (2008) Age-specific interval breast cancers in Japan: estimation of the proper sensitivity of screening using a population-based cancer registry. Cancer Sci 99: 2264–2267
33. D'Orsi CJ, Sickles EA, Mendelson EB et al (2013) ACR BI-RADS atlas; breast imaging reporting and data system. American College of Radiology, Reston VA
34. Lee WJ, Seo BK, Cho PK et al (2010) The clinical use of low-dose multidetector row computed tomography for breast cancer patients in the prone position. J Breast Cancer 13:357–365
35. Wienbeck S, Lotz J, Fischer U (2017) Review of clinical studies and first clinical experiences with a commercially available cone-beam breast CT in Europe. Clin Imaging 42:50–59
36. Taira N, Ohsumi S, Takabatake D et al (2008) Contrast-enhanced CT evaluation of clinically and mammographically occult multiple breast tumors in women with unilateral early breast cancer. Jpn J Clin Oncol 38:419–425
37. Akashi-Tanaka S, Fukutomi T, Miyakawa K et al (2001) Contrast-enhanced computed tomography for diagnosing the intraductal component and small invasive foci of breast cancer. Breast Cancer 8:10–15